NJC

New Journal of Chemistry

A journal for new directions in chemistry

Accepted Manuscript

This article can be cited before page numbers have been issued, to do this please use: A. Goyal, D. Aggarwal, S. Kapoor, N. Goel, S. Singhal and J. Shukla, *New J. Chem.*, 2020, DOI: 10.1039/C9NJ06029D.

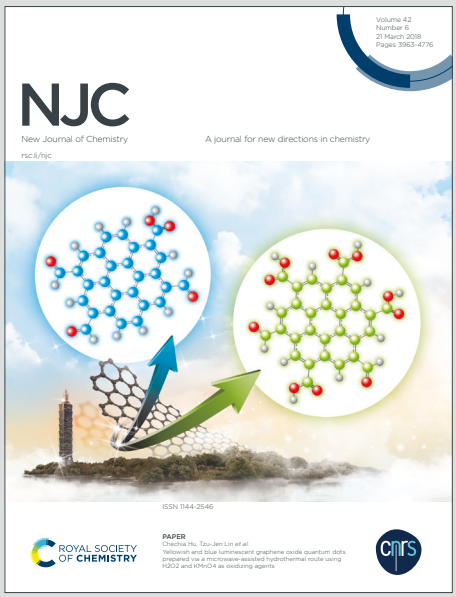

This is an Accepted Manuscript, which has been through the Royal Society of Chemistry peer review process and has been accepted for publication.

Accepted Manuscripts are published online shortly after acceptance, before technical editing, formatting and proof reading. Using this free service, authors can make their results available to the community, in citable form, before we publish the edited article. We will replace this Accepted Manuscript with the edited and formatted Advance Article as soon as it is available.

You can find more information about Accepted Manuscripts in the Information for Authors.

Please note that technical editing may introduce minor changes to the text and/or graphics, which may alter content. The journal's standard Terms & Conditions and the Ethical guidelines still apply. In no event shall the Royal Society of Chemistry be held responsible for any errors or omissions in this Accepted Manuscript or any consequences arising from the use of any information it contains.

View Article Online
DOI: 10.1039/C9NJ06029D

A comprehensive experimental and theoretical study on BN nanosheets for the adsorption of pharmaceutical drugs

Ankita Goyal[a], Diksha Aggarwal[b], Surbhi Kapoor[b], Neetu Goel[b], Sonal Singhal*[b] and Jaya Shukla*[a]

[a]*Department of Nuclear Medicine, PGIMER, Chandigarh-160012, India*

[b]*Department of Chemistry, Panjab University, Chandigarh-160014, India*

Corresponding Authors:

Dr. Jaya Shukla	Dr. Sonal Singhal
Additional Professor Department of Nuclear Medicine and PET Post Graduate Institute of Medical Education and Research Chandigarh 160012 INDIA shuklajaya@gmail.com	Professor Department of Chemistry Panjab Univeristy, Chandigarh 160014 INDIA sonal1174@gmail.com

View Article Online
DOI: 10.1039/C9NJ06029D

Abstract

BN nanomaterials have revolutionized the scientific world with their outstanding physiochemical properties leading to far-fetched applicability in the field of adsorption. In this context, present investigation deals with the synthesis and characterization of BN nanosheets and applicability for the adsorption of pharmaceutical drugs. BN nanosheets exhibited excellent adsorption for Levofloxacin, Tetracycline and Curcumin. To get further insights into the feasibility of adsorption of drugs over BN nanosheets and to scrutinize the interactions between the two, computations have been performed within DFT formalism. The theoretical investigations unveiled the presence of hydrogen bonding and negative adsorption energies liable for favorable adsorption. The synthesized BN nanosheets being biocompatible proved to be proficient adsorbents for the sustainability of environment.

Keywords

Boron nitride, Pharmaceutical drugs, Adsorption Isotherms, Adsorption Kinetics, DFT computations

1. Introduction

Boron nitride (BN) nanomaterials being one of the most promising and popular inorganic nanomaterials are now-a-days furiously reigning the scientific world of applications. This mounting enthusiasm towards the BN nanomaterials is attributed to the chemical structure and properties exhibited by BN at nano level.[1] BN nanomaterials offer excellent physical and chemical properties which make them suitable for a wide variety of applications. The properties include high thermal conductivity, low density, high surface area, presence of structural defects, wide band gap, high pore volume, low thermal expansion, resistance to oxidation, good thermal shock resistance, high electrical resistance, low dielectric constant and loss tangent, microwave transparency, non-toxicity, bio-compatibility, chemical inertness and non-wetting by most molten metals.[2] These unique attributes have dragged the use of BN nanomaterials in a plethora of applications such as surface investigation, composite ceramics, high temperature cooling components, in transistors, protective shielding, high temperature lubricants, cosmetics, gas adsorption, insulation, as catalyst for high temperature treatment, as adsorbents for the removal of

View Article Online
DOI: 10.1039/C9NJ06029D

heavy metal ions, dyes, drugs and other organic pollutants and as drug carriers for in-situ drug delivery.[3–7]

Out of all these areas of interest, the need of adsorbents which are stable, recoverable, reusable, non-toxic, facile to handle; irrespective of the field- whether it is adsorptive removal of pollutants or drug delivery, is budding.[8,9] In this regard, the employment of BN nanomaterials with morphological variations as adsorbents has been the hot area of research lately.[10] Both experimental and theoretical studies have been available in literature wherein adsorption characteristics of BN nanomaterials have been explored with a view of remediation of environmental pollution as well as with the perspective of drug delivery. The features that render BN nanomaterials as potential candidates for adsorption of drugs include high adsorption capacity, high surface area, presence of structural defects, chemical and thermal stability, high chemical inertness and easy cycling ability.[11-14] Different research cohorts have been actively engaged in the production of modified BN nanostructures for the adsorptive removal of different kinds of recalcitrant pollutants.[15–19] Oh *et al.*[15] explored the insights into the adsorption of Cu(II) and Ni(II) on h-BN synthesized at different temperatures-750, 900 and 1050 °C. The sample prepared at 750 °C exhibited the best performance. The adsorbents possessed micro-particle morphology with BET specific surface area between 12–18 m^2g^{-1}. The surface oxygen functional groups (particularly B-O) were found to play an important role in facilitating the electrostatic attraction and complexation of Cu(II) and Ni(II) during adsorption process. Liu *et al.*[16] explored few-layered BN nanosheets synthesized at lower temperature for the adsorption of Pb^{2+}. The process of removal of Pb^{2+} ions was fitted in the pseudo-second order model and Langmuir model, which indicated that it was an endothermic and spontaneous reaction. The equilibrium absorption capacity could get to 845 mg g^{-1} at 25 ºC within 15 min with favourable reusability. Hexagonal boron nitride (BN) bundles formed by the assembly of plenty of BN fibers with high adsorption capacity and outstanding recyclability were explored for the adsorption of sulfadiazine, oxytetracycline and erythromycin antibiotics.[17] Singla *et al.*[18] explored the antibiotic adsorption on the surface of two different morphologies of BN. Two commonly used fluoroquinolones i.e. ofloxacin (OFL) and moxifloxacin (MOXI) were chosen and the adsorption process followed pseudo-second-order kinetic model with good adsorption capacities. Shayan and Nowroozi[19] performed a theoretical investigation on the armchair boron nitride nanotubes (BNNTs) interacting with the 5-fluorouracil (5-FU) (an anticancer drug) using

View Article Online
DOI: 10.1039/C9NJ06029D

B3LYP/6-31G (d,p) level of theory. The encapsulation and adsorption of 5-FU molecule on the studied BNNTs surface was found to be a favorable process, with a few exceptions. BNNTs were established to be considered as a drug delivery vehicle for the transportation of 5-FU as anticancer drug within the biological systems.

Having a view at the above literature, BN nanostructures with different morphologies are extensively being explored for the adsorption of different pollutants as well as drugs. Keeping this in mind, in the present investigation two different types of BN nanosheets- with pores and without pores have been synthesized and explored as adsorbents for two antibiotics belonging to two different classes i.e. Levofloxacin (an anti-bacterial drug belonging to fluoroquinolone family) and Tetracycline (an anti-microbial drug). Additionally, the adsorption of curcumin (Having high therapeutic value against side-effects of chemotherapy) with a view to explore BN for drug delivery application has also been explored. To obtain the best conditions for adsorption, different reaction parameters such as pH, drug loading and adsorbent loading have also been varied. Also, the adsorption kinetics and adsorption isotherms have been explored to acquire the best fit for the obtained data. To get further understanding of the feasibility of adsorption of drugs over BN nanosheets and to examine the interactions between the two, DFT computations have additionally been performed.

2. Experimental

2.1. Materials and reagents

Boric Acid (H_3BO_3, 99.5%), Melamine pure ($C_3H_6N_6$, 99%) and Urea (CH_4N_2O) were purchased from Sigma-Aldrich. Levofloxacin ($C_{18}H_{20}FN_3O_4$, >98%) and Tetracycline Hydrochloride ($C_{22}H_{25}ClN_2O_8$, >98%) were obtained from Tokyo Chemical Industry (TCI) Limited. All chemicals were of analytical grade and used without further purification.

2.2. Fabrication of BN nanosheets

Both the boron nitride nanosheet were prepared using solid state thermal annealing technique with different choice of precursors and different temperature program as discussed below:

2.2.1. Synthesis of BN nanosheets

View Article Online
DOI: 10.1039/C9NJ06029D

In the synthesis of Boron Nitride nanosheets, boric acid and urea were used as the raw materials. A mixture of boric acid and urea was prepared (i.e. in a molar ratio of 1:12) by adding 40 mL of deionized water to the mixture. The mixture was heated at about 65 °C with continuous stirring until it got homogenized and completely dissolved in water. Further, it was heated in an oven at 60°C for 13 h. After the completion of this time, the transparent solution was taken out of the oven and stirred with a glass rod and in few minutes the transparent liquid turned into a white precipitates mass. The dried white compound was further loaded in alumina boats and treated in muffle furnace under continuous flow of nitrogen at 900°C for 5 h. The furnace was allowed to cool and the obtained cooled product was collected, washed with 2M HCl so to remove the impurities, and then dried at about 85 °C for 12 h to obtain BN nanosheets.

2.2.2. Synthesis of porous BN nanosheets

Porous BN nanosheets were prepared using a two-step solid state thermal annealing technique. The first step employed boric acid and melamine as starting materials to obtain the precursor. Typically, boric acid and melamine (2:1 molar ratio) were dissolved in 200 mL of distilled water. The mixture was heated at 85°C for 12 h under continuous stirring and was then allowed to cool down at room temperature. The cooling process turned it in to white flocculated mass. The flocculated mass was filtered and dried at 90 °C for 12 h to obtain a white powder of melamine diborate. In the second step, the white powder was loaded in alumina boats and then treated, first at 300 °C for 1hr and then at 1100 °C for 2 h under continuous flow of N_2. The furnace was allowed to cool down to room temperature and then the product was collected from the alumina boats followed by washing with 2M HCl to remove the impurities. The pure product was finally dried at about 85 °C for 12 h to obtain porous BN nanosheets.

Also, the formation of pores during the synthesis of porous BN nanosheets could be accounted to the use of melamine as N-containing precursor (source of nitrogen). The thermal decomposition of melamine led to the release of various gases that could result in the formation of porous structure.[20] But in the synthesis of BN nanosheets, urea was used as N-containing precursor and it is well evident from the previous literature report that the porosity of BN nanosheets remained limited in case of employment of urea as precursor.[21]

2.3. Procedure for adsorption and release of drugs

View Article Online
DOI: 10.1039/C9NJ06029D

In order to examine the adsorption ability of the synthesized BN nanomaterials, adsorption studies were carried out for the adsorption of antibiotic drugs (Levofloxacin and Tetracycline) and Curcumin. The aqueous stock solution was prepared with 50 mg/L concentration. For the adsorption experiments, 100 mL of antibiotic solution with known concentration was taken in 250 mL beaker to which desired amount of adsorbent was added. The adsorption reaction started at once with the addition of adsorbent into the drug solution which was continuously stirred using magnetic bar on magnetic stirrer. Subsequent sample aliquots were taken after fixed time intervals and adsorbent was removed using centrifugation. UV-visible spectroscopy was then employed for obtaining the corresponding concentration of the drug solution. The effect of different reaction variables such as pH, drug concentration, adsorbent dosage and time of contact has also been evaluated.

The procedure for the release of drugs involves the dispersion of 10 mg of BN-drug complex in 10 mL PBS buffer solution at different pH values (2, 6 and7.4). At different time intervals, 3 mL aliquots of PBS solution were collected and centrifuged to obtain clear supernatant solution. The concentrations of the released drug were analyzed using UV-visible spectral measurement. Further, 3 mL of fresh PBS buffer was added back to retain the initial volume of the solution.[22]

2.4. Physical Measurements

The knowledge of different kinds of bonds present and their vibrational modes was acquired using iS50-FTIR (Fourier transform infra-red spectroscopy (FT-IT)) (Model no. AUP1200343) instrument with the resolution of 1 cm^{-1} and scan range of 4000 cm^{-1} to 400 cm^{-1}. The details of the structural aspects, knowledge of type of crystal lattice, corresponding lattice planes and space-group was attained using powder X-ray diffraction (XRD) technique. Panalytical's X'Pert Pro diffractometer equipped with vertical theta-theta goniometer and x'Celerator solid-state detector, was employed for recording the XRD pattern of the powdered sample. Shape, size, morphology and elemental composition of the synthesized BN nanostructures were examined using Field emission scanning electron microscopy (FESEM) employing Hitachi (SU-8010) operated at 15 kV. EDS and elemental mapping were also done using the attached accessory with FESEM instrument. High resolution transmission electron microscopy (HR-TEM- FEI Tecnai (G2 F20) operating at 200 keV) further confirmed the shape and size and provided information about the

View Article Online
DOI: 10.1039/C9NJ06029D

crystallinity and different lattice planes. X-ray photoelectron microscopy (XPS) analysis was carried out using ESCA+, (omicron nanotechnology, Oxford Instrument Germany) equipped with monochromator Aluminum Source (Al kα radiation hυ =1486.7eV) operated at 15 kV and 20 mA. For the absorbance measurements, JASCO V-750 spectrophotometer was employed. For the estimation of surface area, BET method was employed and calculation was done using Belsorp max. To acquire the charge present on the surface of BN, Zeta potential instrument was employed.

2.5. Computational Methodology

DFT calculations were employed for the validation of feasibility of adsorption and better understanding of principle interactions between drugs and BN nanosheet. The geometrical optimization of drugs and BN nanosheet was carried out by hybrid generalized gradient approximation i.e. Becke, 3-parameter, Lee–Yang–Parr (B3LYP)[23,24] in conjunction with 6-31G basis set as implemented in Gaussian 09 simulation package.[25] The vibrational frequency analysis was also performed for the confirmation of the optimized geometries as minima (no imaginary frequency). The adsorption energy (E_{ads}) of drug adsorbed over BN nanosheet was calculated as:

$$E_{ads} = E_{adsorbate+adsorbent} - (E_{adsorbate} + E_{adsorbent}) \quad (1)$$

where, $E_{adsorbate+adsorbent}$, $E_{adsorbate}$ and $E_{adsorbent}$ represents the total energy of drug adsorbed over BN nanosheets, energy of drug and energy of BN nanosheet, respectively. The exothermic nature of the adsorption is governed by negative adsorption energy ($E_{ads} < 0$).

3. Results and discussion

3.1. Structural and Morphological Characterization

For the confirmation of successful formation of the BN nanostructures, FT-IR spectra were recorded. In the FT-IR spectra (Fig. 1.) for porous BN and BN nanosheets, two characteristic peaks corresponding to BN bonding were observed. Strong asymmetric band appeared at 1365 cm^{-1} and 768 cm^{-1} corresponding to in-plane B-N transverse optical mode of sp^2-bonded h-BN and B-N-B out of plane bending vibrations, respectively, were observed. An additional broad band in the range of 3400-3200 cm^{-1} was also observed owing to the –OH groups present in the adsorbed H_2O molecules.[26]

The structural characteristics of adsorbents were observed using powder XRD analysis. The XRD patterns (Fig. 2.) for porous BN and BN nanosheets matched well with standard

View Article Online
DOI: 10.1039/C9NJ06029D

patterns[27] corresponding to pure h-BN with P63/mmc space group (JCPDS no. 34-0421). Peaks corresponding to six major planes i.e. (0 0 2), (1 0 0), (1 0 1), (0 0 4), (1 1 0) and (1 1 2) were observed at 2θ positions of 27.16°, 41.59°, 43.87°, 55.16°, 75.93° and 82.17° respectively. It was observed that the intensity of peaks corresponding to BN nanosheet was lower in comparison with porous BN. The lower intensity of peaks of BN nanosheet could be ascribed to the BN disorder or defect density.[28,29] Also, the difference in intensity of peaks of BN nanosheet and porous BN could also be attributed to the variance in the temperature range employed in the synthesis procedure. It is known from the previous literature reports that increase in temperature results in the increase in peak intensity.[30,31] The processing temperature used in the preparation of BN nanosheet was quite lower in comparison with that used in the synthesis of porous BN that could account for the lower intensity of peaks corresponding to BN nanosheet. The values of lattice parameters "a" and "c" were calculated using Le-Bail refinement method and crystallite size was appraised from the line broadening of the most intense peak observed at 2θ position of 27.16° for (0 0 2) plane and are given in Table. 1.

FE-SEM studies revealed the morphological characteristics of the BN nanostructures. Low resolution FE-SEM images (Fig. 3 (a) and (d)) for both BN nanostructures confirmed the formation of sheet like structures. Further magnification revealed that in one case (for the case of porous) there are pores present on the surface while for other pores were not there as confirmed from Fig. 3 (b) and (e), respectively. The samples were further observed at higher resolution (Fig. 3 (c) and (f)) and were found to be made up of very minute quasi-spherical particles with size in the range of 10-15 nm.

HR-TEM data obtained for Porous BN and BN nanosheets have been given in Fig. 4 and Fig. 5, respectively. Fig. 4 (a) and (b) depict the low resolution TEM images showcasing the minute quasi-spherical particles gathered together forming the porous structure. Fig. 4 (c) and (d) are the high resolution TEM images showing the interplanar distance corresponding to different lattice planes present in the structure. The interplanar spacing (0.33 nm) corresponding to most intense peak (0 0 2) as observed in XRD has been marked. Fig. 5 (a) and (b) display the presence of tightly packed spherical particles forming sheet like structure. Fig. 5 (c) shows the interplanar spacing corresponding to the most intense peak as observed in XRD. Fig. 4 (e) and Fig. 5 (d) are the SAED patterns which display concentric electron diffraction rings obtained corresponding to electron

View Article Online
DOI: 10.1039/C9NJ06029D

density present in different planes, marked in the images. EDS patterns (Fig. 4 (f) and 5 (e)) show the presence of B, C, N, O and Cu. C and Cu have been observed owing to the use of C coated Cu grid for the measurement.

The purity of the synthesized BN nanostructures was further supported by XPS spectroscopy. The XPS spectra for both the BN nanostructures have been shown in Fig. 6 and Fig. 7. The peaks corresponding to B1s, C1s, N1s and O1s were observed to be there. C and O emerged in the spectrum owing to the XPS measurement.[32] The observed binding energies for B and N were in close agreement corresponding to hexagonal BN reported in literature.[33] The B/N ratio from the XPS survey for porous BN and BN nanosheet were observed to be 1.03 and 1.05, respectively.

3.2. Surface Area and Surface Charge studies

The Brunauer-Emmett-Teller (BET) N_2 adsorption/desorption measurements were performed to determine the surface area. The N_2 adsorption/desorption isotherms for porous BN and BN nanosheets matched with type IV and type I adsorption isotherms, respectively (Fig. 8 (a) and (b)). These adsorption isotherms depict monolayer adsorption for BN nanosheet and monolayer adsorption at low pressure and multilayer adsorption at high pressure for porous BN nanosheet. Type IV BET isotherm is observed for porous BN which suggests the predominance of mesoporous structure. The presence of mesopores could lead to a greater enhancement in the adsorption capacity. Also, the persistence of the capillary condensation effect in case of Type IV isotherm also plays its role that could lead to an addition better adsorption. [34-35]

The BET adsorption relation is given by equation (2).[36] 'P' and 'P_0' are the equilibrium and saturation pressure, 'Q' is the quantity of the gas adsorbed on the adsorbate, 'Q_m' is the monolayer adsorbed gas quantity and 'C' is the BET constant.

$$\frac{1}{Q\left[\left(\frac{P_0}{P}\right)-1\right]} = \frac{C-1}{Q_m C}\left(\frac{P}{P_0}\right) + \frac{1}{Q_m C} \qquad (2)$$

According to equation (2) graphs were plotted between $1/[Q\{(P_0/P)-1\}]$ vs. P/P_0 named as BET adsorption isotherm (Fig. 8(c) and (d)). From the plot the values of slope (A) and intercept (I) were deduced and the values of 'Q_m' and 'C' were calculated according to the equations (3) and (4).

View Article Online
DOI: 10.1039/C9NJ06029D

$$Q_m = \frac{1}{A + I} \quad (3)$$

$$C = 1 + \frac{A}{I} \quad (4)$$

Further, the values of Total surface area (S_{total}) and Specific surface area (S_{BET}) were calculated according to the equations (5) and (6).

$$S_{total} = \frac{Q_m N s}{V} \quad (5)$$

$$S_{BET} = \frac{S_{total}}{M} \quad (6)$$

Where, 'N' is Avogadro's number, 's' (0.1620 nm^2) is molecular cross-sectional area, 'V' is the molar volume of the adsorbate gas and 'M' is the mass of the adsorbent sample. The value of Q_m, C, M, S_{total} and S_{BET} for both the samples have been included in Table. 2.

The surface charge is very crucial parameter that could facilitate the knowledge of the type of adsorbate to be absorbed. To gain this idea, Zeta potential analysis was performed for both the BN nanomaterials. For the surface charge measurement, the medium used was water at neutral pH. A constant voltage (3.4 V) was applied between the electrodes placed in the dispersion medium and conductivities of both the BN nanomaterials were measured depicting the zeta potential values to be -25.5 mV and -22.8 mV for porous BN and BN nanosheets respectively. The negative values of the zeta potential demonstrate the presence of negative charge on their surface.

The characterization results revealed that both the BN nanostructures were obtained in pure form with well-defined structural characteristics, high surface area and possess negative charge on their surface. Further, the adsorption characteristics were explored for both the BN nanostructures.

3.3. Adsorption Studies

For the evaluation of the adsorption characteristics of the synthesized BN nanostructures, adsorption of Levofloxacin and Tetracycline as model compounds was carried out. The time dependent progress of the adsorption reaction was evaluated using UV-visible spectroscopy. Levofloxacin which is an antibiotic belonging to fluoroquinolone family exhibits absorption maxima at ~293 nm in the UV-visible range and Tetracycline which is an antibiotic used to fight against bacterial infections exhibits absorption maxima at ~381 nm. The absorption maxima were

View Article Online
DOI: 10.1039/C9NJ06029D

found to decrease with the passage of time for both the drugs with both the BN nanostructures under chosen experimental conditions, indicating their potential towards adsorptive removal. Also, to evaluate the effect of different pH conditions, initial drug concentration and adsorbent dosage, a series of adsorption experiments were performed. The initial pH has been varied from 2 to 10 with fixed adsorbent dosage (1 g/L) and drug loading of 10 mg/L for Levofloxacin and 50 mg/L for Tetracycline. It can be inferred that maximum adsorption could be obtained at pH=4 with an adsorption % of 96.4% for porous BN and 94.1% for BN nanosheets for Levofloxacin, while, for Tetracycline it was maximum at pH-6 with 84.2% for porous BN and 82.7% for BN nanosheets. Also, the drug dosage has been varied for both the BN nanostructures and it was found that drug dosage of 10 mg/L for Levofloxacin and 50 mg/L for Tetracycline exhibited the best results. The adsorbent dosage of 1g/L was found to be optimum for both the drugs and for both the BN nanostructures. The obtained results have been given in Fig. S1 and S2 and Fig. S3 respectively (supporting information). After obtaining the optimum conditions adsorption kinetics and adsorption isotherms were explored.

The kinetic study of adsorption plays a very important aspect of adsorption process as it gives an idea of adsorbate uptake rate, adsorption efficiency and feasibility. For detailed analysis for the adsorption data several kinetic models have been used in the literature.[37]

Here, in this work two kinetic models have been evaluated i.e. pseudo-first-order and pseudo-second-order. Pseudo first order kinetics equation is:

$$\log\left(q_e - q_t\right) = \log q_e - \frac{k_1}{2.303}t \qquad (7)$$

where q_e and q_t are the adsorption capacities (mg g^{-1}) at equilibrium and at time t, respectively, while k_1 is the pseudo-first-order rate constant (min^{-1}). The slope and intercept of linear plot of log (q_e - q_t) *vs.* t (Fig. S4) were used to evaluate the values of k_1 and q_e respectively.

The pseudo-second-order model depicts the variation of adsorption rate with adsorption capacities and is formulated as:

$$\frac{t}{q_t} = \frac{1}{k_2 {q_e}^2} + \frac{t}{q_e} \qquad (8)$$

where k_2 is the pseudo-second-order rate constant (g $mg^{-1}min^{-1}$). The values of q_e and k_2 can be obtained from the linear plot of t/q_t *vs.* t via deducing the slope and intercept respectively (Fig.

View Article Online
DOI: 10.1039/C9NJ06029D

S5). The data obtained from the kinetic plots is tabulated in Table. 3. By comparing the correlation coefficient (R^2) values, pseudo-second-order kinetic model exhibited good agreement between the experimental and calculated values and correctly described the adsorption kinetics via having higher R^2 values as compared to first order kinetic model.

The study of adsorption isotherms is very helpful to understand the feasibility of an adsorbate-adsorbent system.[38] In this work, Langmuir and Freundlich adsorption isotherm models were used for the interpretation of the experimental data. In order to determine the adsorption isotherm, adsorbent dosage of 1g/L was used under the optimized experimental conditions with varying drug dosage. The linear representation of the Langmuir isotherm model can be expressed as follow:[39,40]

$$\frac{C_e}{q_e} = \frac{1}{q_{max}K_L} + \frac{C_e}{q_{max}} \quad (9)$$

where q_{max} and K_L are Langmuir constants related to maximum adsorption capacity of adsorbents (mg/g) and Langmuir adsorption constant (L/mg), also known as effective dissociation constant, respectively, while C_e and q_e represent the drug concentration (mg/L) and adsorption capacity (mg/g) at equilibrium, respectively. From the linear plot between (C_e/q_e) against C_e (Fig. S6), values of the Langmuir constants i.e. q_{max} and K_L were determined from the slope and intercept and listed in Table. 4. The essential characteristic of the Langmuir isotherm is the dimensionless constant called equilibrium parameter (R_L) and it can be expressed as follows:[41]

$$R_L = \frac{1}{1 + K_L C_o} \quad (10)$$

where C_o is the initial drug concentration in (mg/L). Depending upon the value R_L, adsorption is considered to be unfavorable ($R_L > 1$), linear ($R_L = 1$), favorable ($0 < R_L < 1$), or irreversible ($R_L = 0$). It was found that value of R_L for both the drugs is between 0 and 1, depicting favorable adsorption.

The mathematical representation of the Freundlich isotherm model is as follows:

$$logq_e = logK_F + \frac{logC_e}{n} \quad (11)$$

View Article Online
DOI: 10.1039/C9NJ06029D

where K_F ((mg/g) $(L/mg)^{1/n}$) and n are Freundlich constant representing the adsorption capacity of the adsorbent and the energy of adsorption effectiveness, respectively. The values of K_F and n are calculated from the intercept and the slope of the plot of log q_e *vs.* log C_e (Fig. S7) are tabulated in Table. 4. The R^2 values from two kinds of adsorption isotherms are summarized in Table. 4 and it indicates that the experimental adsorption equilibrium data of the system data fit the Langmuir isotherm better as it had significantly higher correlation coefficient in comparison to Freundlich isotherm. Therefore, it is imputed from the results that the adsorption of drugs takes place in a monolayer manner over the surface of both BN nanostructures. Further, the maximum adsorption capacities attained for Levofloxacin and Tetracycline as calculated from Langmuir plots were 17.6056 mg g^{-1} and 129.8700 mg g^{-1}, respectively, employing 1g/L porous BN; and 20.0803 mg g^{-1} and 86.206, respectively, employing 1g/L BN nanosheet.

The adsorption studies revealed that for both the BN nanostructures and for both the drugs the adsorption R_L values lies between 0 and 1, suggesting favorable adsorption. For both the BN nanostructures, the best results for Levofloxacin were observed at pH-4 followed by pH-6. Levofloxacin exist in cationic form below pH-5 and at pH-6 it exist in zwitter-ionic form. As the surface of BN nanostructures possess negative charge maximum adsorption could be expected at pH-2, but at pH-2, H^+ present in the reaction mixture start competing with drug molecules thus, lowering the adsorption of drug.[42]

For Tetracycline, best results for both the BN nanostructures were observed at pH-6 followed by pH-4. At pH-6, Tetracycline exist in zwitter-ionic form, at pH less than 4, it exist in cationic form. The best results at pH-6 could be related to the dominant π-π interaction mechanism.[43]

Having a view on the adsorption results obtained for the adsorption of both the drugs on the surface of both the BN nanosheets, it was inferred that better results were obtained for porous BN nanosheets. So it was further decided to explore porous BN nanosheets for the adsorption of curcumin on its surface. Curcumin has been chosen based upon its therapeutic action against the side-effects of chemotherapy. It is safe to intake curcumin with a dosage of 8 g/day for patients undergoing chemotherapy. But curcumin when undertaken directly it decomposes or degrades before its therapeutic action owing to its sensitivity towards elevated temperature, basic pH and exposure to light and insolubility in aqueous medium.[44,45] So an attempt has been made to stabilize

View Article Online
DOI: 10.1039/C9NJ06029D

it via its adsorption over some solid surface to increase its bio-availability. Prior to adsorption studies, different reaction parameters (pH, adsorbent dosage, drug concentration) were optimized to explore the best conditions for adsorption. Three acidic pH were tested i.e. 1, 3 and 5. Alkaline pH values were not explored owing to the instability of curcumin in alkaline medium. Adsorbent dosage has been varied from 50 mg to 125 mg and drug concentration has been varied from 5 mg/L to 50 mg/L. The variation of pH, adsorbent dosage and drug concentration for the adsorption of curcumin over the surface of porous BN nanosheet has been shown in Fig. S8. It was observed that percent adsorption was found to be maximum at pH-5. The percent adsorption was found to increase with increase in adsorbent dosage and it decreased with increase in drug dosage. This could be related to the fact that with increase in adsorbent dosage number of available adsorption sites got increased and with increase in drug dosage number of molecules to be adsorbed on the same number of sites got increased thus, decreasing the adsorption. Further, adsorption kinetic and adsorption isotherms for the adsorption of curcumin over the surface of porous BN nanosheets were explored as per the prior discussed equations-equation (1-5). For the understanding of adsorption kinetics and adsorption isotherms, pseudo-first-order and pseudo-second-order kinetic models and Langmuir and Freundlich adsorption isotherms were explored (Fig. S9 and Fig. S10). The adsorption was found to follow pseudo-second order kinetics and fitted well with Langmuir adsorption isotherm.[46,47] The corresponding values of rate constants and correlation co-efficients and adsorption parameters have been given in Table. 4. The maximum adsorption capacity attained for Curcumin as calculated from Langmuir plot was 32.3620 mg g^{-1} employing 1g/L porous BN.

3.4. Release studies

To examine in vitro drug release, porous BN-Levofloxacin complex was dispersed in PBS buffer at different pH (2, 6 and 7.4) for 48 h. The above pH values were selected in accordance with the pH of stomach (1.5-3.5) and normal tissue and blood (7.4).[46] Further, UV-visible spectrophotometric measurements of Levofloxacin concentrations were performed and the release kinetics is represented in Fig. 9. It was clearly visualized that the release of Levofloxacin from porous BN-Levofloxacin complex was pH-responsive. At pH 2, around 19% Levofloxacin was released within 48 h. On the other hand, at pH values of 6 and 7.4, around 35% and 62% of loaded Levofloxacin were released in 48 h, respectively. Thus, the release rate was found to increase with increase in the pH value. The enhanced Levofloxacin release from porous BN-Levofloxacin

View Article Online
DOI: 10.1039/C9NJ06029D

complex at 7.4 could be attributed to the change in electrostatic interactions between porous BN nanosheet and Levofloxacin.[48,49,50]

3.5. Theoretical studies

To investigate the interactions between drugs and BN nanosheet and to determine the adsorption energies, calculations were performed using DFT framework. Prior to the adsorption studies, the geometries of antibiotic drugs (Levofloxacin and Tetracycline) and Curcumin were optimized and are represented in Fig. S11. Also, the optimized geometry of finite sized BN nanosheet consisting of 36 boron atoms and 36 nitrogen atoms in hexagonal manner was modeled as representative of both porous BN and BN nanosheets where open ends were saturated with hydrogen atoms (Fig. S12). Further, the adsorption of above drugs on BN nanosheet was investigated separately and the most stable configurations are shown in Fig. 10. It is well evident that when the sum of van der Waals radii of constituent atoms is greater than bond length, it signifies the presence of hydrogen bonding. In the present case, hydrogen bond was formed between hydrogen atom present in drugs and nitrogen of BN nanosheet. The sum of van der Waals radii of hydrogen (0.12 Å) and nitrogen (0.155 Å) i.e. 0.275 Å was found to be greater than bond lengths i.e. 2.61 Å (levofloxacin), 2.16 Å (tetracycline) and 2.32 Å (curcumin). This convection revealed the presence of hydrogen bonding between drugs and BN nanosheet. Also, the oxygen present in the drug molecules was at a close proximity with boron of BN nanosheet signifying the interactions between the atoms due to their partial opposite charges. The distances between oxygen and boron atoms were observed to be 2.96 Å, 2.89 Å and 2.95 Å for levofloxacin, tetracycline and curcumin, respectively. In the case of adsorption of curcumin over BN nanosheet, stacking interactions between the rings were also observed. The adsorption energies of drugs adsorbed on BN nanosheet as calculated by equation (1) were observed to be -0.76 eV (Levofloxacin), -0.79 eV (Tetracycline) and -0.60 eV (Curcumin). The negative adsorption energies unveiled the exergonic nature and thermodynamic favorability of adsorption process. The order of adsorption energies of drugs on BN nanosheet was found to be Tetracycline > Levofloxacin > Curcumin. Molecular electrostatic potential (MEP) surfaces were also generated for the better understanding of adsorption of drugs over BN nanosheet (Fig. 11). The merging of charge clouds of drugs and BN nanosheet was clearly visualized depicting the affinity of BN nanosheet towards drug molecules. Also, the interactions between hydrogen of drug and nitrogen of BN nanosheet; and electronegative oxygen or fluorine of drug and electropositive boron were observed by analyzing

View Article Online
DOI: 10.1039/C9NJ06029D

the overlapping areas. Thus, MEP surfaces also accounted for the interactions between drugs and BN nanosheet for the favorable adsorption.

Both the experimental results and theoretical calculations validated both the BN nanosheets as high potential candidates for the rapid and effective adsorption of pharmaceutical drugs with a view to fight against the pollution menace and infections via drug delivery.

3.6. Recyclability

In order to establish the reusability and stability of BN nanostructures, recyclability experiments were performed for the adsorptive removal of Levofloxacin under the optimized experimental conditions using porous BN as adsorbent. After the complete adsorption, Levofloxacin adsorbed BN was separated from the reaction mixture using centrifugation and the obtained pellet was dried in an oven at 80 °C for 10 hr. To remove the adsorbed drug, the BN nanostructures were annealed at 500 °C for 1 hr. The obtained BN nanostructures were then repeatedly used for the proceeding experiments. The recyclability was established up to 3 cycles without any significant loss in the adsorption capability, while, for the fourth cycle a slight decrease in adsorption capacity was there. The recyclability results have been shown in Fig. 12.

Further, characterization of recovered adsorbents (porous BN and BN nanosheet) was done and the results were compared with the adsorbents before drug adsorption. The structure of the recovered adsorbents was examined using XRD (Fig. 13(a)) and FT-IR analysis (Fig. 13(b)). The XRD patterns and FT-IR spectra demonstrated that the structure of the adsorbents remained unchanged after recycling when compared with the adsorbents before drug adsorption indicating high stability of the adsorbents. Also, the morphology of the recovered porous BN and BN nanosheet was scrutinized by FE-SEM analysis that revealed no change in the surface morphology of the recovered adsorbents (Fig. 14). Thus, the post reaction analysis established that the synthesized adsorbents displayed excellent stability during adsorption processes.

Conclusions

Porous BN and BN nanosheets were successfully explored as high performance adsorbents for pharmaceutical drugs. The adsorption of drugs was fitted well in the pseudo-second-order kinetic model and Langmuir model. The porous BN nanosheets were observed to be superior adsorbents in comparison with BN nanosheets and displayed adsorption capacities of 17.61 mg

View Article Online
DOI: 10.1039/C9NJ06029D

g^{-1}, 129.87 mg g^{-1} and 32.36 mg g^{-1} for Levofloxacin, Tetracycline and Curcumin, respectively. DFT computations further demonstrated the presence of interactions between adsorbed drugs and BN nanosheet accountable for favorable adsorption. Also, the negative adsorption energies unveiled the exothermic and thermodynamically favorable nature of adsorption. Thus, the present study offers insightful prospective for the employment of BN nanosheets as potential candidates for the environmental sustainability as well as for drug delivery.

Conflicts of interest

There are no conflicts of interest.

Acknowledgement

The authors are highly thankful to Post graduate Institute of Medical Education and Research, Chandigarh (Endst No.71/2-Edu-16/161-62) and SERB-NPDF (PDF/2017/000423) for the required financial support.

References

1. S. Yu, X. Wang, H. Pang, R. Zhang, W. Song, D. Fu, T. Hayat and X. Wang, *Chem. Eng. J.*, 2018, **333**, 343–360.
2. X.F. Jiang, Q. Weng, X.B. Wang, X. Li, J. Zhang, D. Golberg and Y. Bando, *J. Mater. Sci. Technol.*, 2015, **31**, 589–598.
3. Y. He, D. Li, W. Gao, H. Yin, F. Chen and Y. Sun, *Nanoscale*, 2019, **11**, 21909–21916.
4. C.C. Cheng, A.A. Muhabie, S.Y. Huang, C.Y. Wu, B.T. Gebeyehu, A.W. Lee, J.Y. Lai and D.J. Lee, *Nanoscale*, 2019, **11**, 10393–10401.
5. W.D. Oh, M.G.H. Lee, W.C. Udayanga, A. Veksha, Y. Bao, A. Giannis, J.W. Lim and G. Lisak, *J. Environ. Chem. Eng.*, 2019, **7**, 102872.
6. X. Mao, S. Zhou, C. Yan, Z. Zhu and A. Du, *Phys. Chem. Chem. Phys.*, 2019, **21**, 1110–1116.
7. M.B. Jakubinek, B. Ashrafi, Y. Martinez-Rubi, J. Guan, M. Rahmat, K.S. Kim, S. Dénommée, C.T. Kingston and B. Simard, *Boron Nitride Nanotube Composites and Applications*, William Andrew Publishing, Nanotube Superfiber Materials, 2019.
8. R.S. Bangari and N. Sinha, *J. Mol. Liq.*, 2019, **293**, 111376.
9. E. Duverger, S. Balme, M. Bechelany, P. Miele and F. Picaud, *Appl. Surf. Sci.*, 2019, **475**, 666–675.

View Article Online
DOI: 10.1039/C9NJ06029D

10. W. Li, H. Yang, S. Chen, Q. Chen, L. Luo, J. Li, Y. Chen and C. Li, *J. Nanomater.*, 2019, https://doi.org/10.1155/2019/3572317.
11. J. Pang, Y. Chao, H. Chang, H. Li, J. Xiong, M. He, Q. Zhang, H. Li and W. Zhu, *J. Colloid Interface Sci*., 2017, **508**, 121-128.
12. Q. Li, T. Yang, Q. Yang, F. Wang, K.C. Chou and X. Hou, *Ceram. Int.*, 2016, **42**, 8754-8762.
13. H. Wang, W. Wang, H. Wang, F. Zhang, Y. Li and Z. Fu, *Ceram. Int.*,2018, **44**, 12216-12224.
14. Q. Song, Y. Fang, Z. Liu, L. Li, Y. Wang, J. Liang, Y. Huang, J. Lin, L. Hu, J. Zhang and C. Tang, *Chem. Eng. J*., 2017, **325**, 71-79.
15. W.D. Oh, M.G.H. Lee, W.C. Udayanga, A. Veksha, Y. Bao, A. Giannis, J.W. Lim and G. Lisak, *J. Environ. Chem. Eng.*, 2019, **7**, 102872.
16. T. Liu, Y. Li, J. He, K. Zhang, Y. Hu, X. Chen, C. Wang, X. Huang, L. Kong and J. Liu, *J. Mater. Sci.*, 2019, **54**, 5366–5380.
17. Q. Song, J. Liang, Y. Fang, C. Cao, Z. Liu, L. Li, Y. Huang, J. Lin and C. Tang, *J. Hazard. Mater.*, 2019, **364**, 654–662.
18. P. Singla, N. Goel and S. Singhal, *Ceram. Int.*, 2015, **41**, 10565–10577.
19. K. Shayan, and A. Nowroozi, *Appl. Surf. Sci.*, 2018, **428**, 500–513.
20. S. Marchesini, C.M. McGilvery, J. Bailey and C. Petit, *ACS Nano*, 2017, **11**, 10003–10011.
21. A. Nag, K. Raidongia, K.P. Hembram, R. Datta, U.V. Waghmare and C.N.R. Rao, *ACS Nano*, 2010, **4**, 1539–1544.
22. L. Xu, Y. Xue, J. Xia, X. Qu, B. Lei, T. Yang, X. Zhang, N. Li, H. Zhao, M. Wang and M. Luo, *Biomaterials*, 2020, **230**, 119670.
23. A. D. Becke, *J. Chem. Phys.*, 1993, **98**, 5648–5652.
24. C. Lee, W. Yang and R. G. Parr, *Phys. Rev. B*, 1988, **37**, 785–789.
25. M. J. Frisch, G. W. Trucks, H. B. Schlegel, G. E. Scuseria, M. A. Robb, J. R. Cheeseman, G. Scalmani, V. Barone, B. Mennucci, G. A. Petersson, H. Nakatsuji, M. Caricato, X. Li, H. P. Hratchian, A. F. Izmaylov, J. Bloino, G. Zheng, J. L. Sonnenberg, M. Hada, M. Ehara, K. Toyota, R. Fukuda, J. Hasegawa, M. Ishida, T. Nakajima, Y. Honda, O. Kitao, H. Nakai, T. Vreven, J. A. Montgomery, Jr., J. E. Peralta, F. Ogliaro, M. Bearpark, J. J. Heyd, E. Brothers, K. N. Kudin, V. N. Staroverov, R. Kobayashi, J. Normand, K. Raghavachari, A. Rendell, J. C. Burant, S. S. Iyengar, J. Tomasi, M. Cossi, N. Rega, J. M. Millam, M. Klene, J. E. Knox, J. B. Cross, V. Bakken, C. Adamo, J. Jaramillo, R. Gomperts, R. E. Stratmann, O. Yazyev, A.

View Article Online
DOI: 10.1039/C9NJ06029D

J. Austin, R. Cammi, C. Pomelli, J. W. Ochterski, R. L. Martin, K. Morokuma, V. G. Zakrzewski, G. A. Voth, P. Salvador, J. J. Dannenberg, S. Dapprich, A. D. Daniels, Ö. Farkas, J. B. Foresman, J. V. Ortiz, J. Cioslowski, and D. J. Fox, Gaussian, Inc., Wallingford CT, Gaussian 09, Revision E.01, 2009.

26. L. Chen, M. Zhou, Z. Luo, M. Wakeel, A. Asiri and X. Wang, *Appl. Catal., B*, 2019, **241**, 246–255.
27. A. Ozkan, N. Atar and M. Yola, *Biosens. Bioelectron.*, 2019, **130**, 293–298.
28. R. Que, Y. Huang, Q. Li, H. Yao, B. Geng and M. Shao, *ACS Appl. Mater. Interfaces*, 2014, **6**, 19752–19757.
29. Y. Lin, T.V. Williams, W. Cao, H.E. Elsayed-Ali and J.W. Connell, *J. Phys. Chem.* C, 2010, **114**, 17434–17439.
30. D. Saha, G. Orkoulas, S. Yohannan, H.C. Ho, E. Cakmak, J. Chen and S. Ozcan, *ACS Appl. Mater. Interfaces*, 2017, **9**, 14506–14517.
31. N. Kostoglou, J. Lukovic, B. Babic, B. Matovic, D. Photiou, G. Constantinides, K. Polychronopoulou, V. Ryzhkov, B. Grossmann, C. Mitterer and C. Rebholz, *Mater. Des.*, 2016, **110**, 540–548.
32. M. Du, Y. Wu and X. Hao, *Cryst. Eng. Comm.*, 2013, **15**, 1782–1786.
33. H. Li, S. Zhu, M. Zhang, P. Wu, J. Pang, W. Zhu, W. Jiang, H. Li, *ACS Omega*, 2017, **2**, 5385–5394.
34. M. Ghasemi, H. Javadian, N. Ghasemi, S. Agarwal and V.K. Gupta, *J. Mol. Liq.*, 2016, **215**, 161-169.
35. M. Khalfaoui, S. Knani, M.A. Hachicha and A.B. Lamine, *J. Colloid Interface Sci*., 2003, **263**, 350-356.
36. A. Goyal, S. Bansal, P. Samuel, V. Kumar and S. Singhal, *J. Mater. Chem. A*, 2014, **2**, 18848–18860.
37. M. Jianzhe, L. Yang, A. Muhammad, W. Fengyun, C. Yuting, L. Wu, X. Mingzhu and Z. Sidi, *Int. J. Biol. Macromol.*, 2019, **124**, 557–567.
38. X. Hu, L. Jia, J. Cheng and Z. Sun, *J. Hazard. Mater.*, 2019, **362**, 1–8.
39. W. He, X. Guo, J. Zheng, J. Xu, T. Hayat, N.S. Alharbi and M. Zhang, *Inorg. Chem.*, 2019, **58**, 7255–7266.

View Article Online
DOI: 10.1039/C9NJ06029D

40. J. Zheng, M. Zhang, T. Miao, J. Yang, J. Xu, N.S. Alharbi and M. Wakeel, *Mater. Chem. Front.*, 2019, **3**, 224–232.
41. R. Gao, Y. Hao, L. Zhang, X. Cui, D. Liu, M. Zhang, Y. Tang and Y. Zheng, *Chem. Eng. J.*, 2016, **284**, 139–148.
42. X. Qin, F. Liu, G. Wang, L. Weng and L. Li, *Colloids Surf., B*, 2014, **116**, 591–596.
43. Y. Gao, Y. Li, L. Zhang, H. Huang, J. Hu, S. Shah and X. Su, *J. Colloid. Interface Sci.*, 2012, **368**, 540–546.
44. A. Duvoix, R. Blasius, S. Delhalle, M. Schnekenburger, F. Morceau, E. Henry, M. Dicato and M. Diederich, *Cancer Lett.*, 2005, **223**, 181–190.
45. R.M. Srivastava, S. Singh, S.K. Dubey, K. Misra and A. Khar, *Int. Immunopharmacol.*, 2011, **11**, 331–341.
46. N. Wang, M. Zhang, L. Liu, J. Zheng, J. Xu, T. Hayat and N.S. Alharbi, *Nanotechnology*, 2019, **30**, 415602.
47. M. Zhang, T. Miao, J. Zheng, J. Xu, A.M. Asiri and H.M. Marwani, *Microporous Mesoporous Mater.*, 2019, **286**, 207–213.
48. S. Feng, H. Zhang, C. Zhi, X.D. Gao and H. Nakanishi, *Int. J. Nanomedicine*., 2018, **13**, 641.
49. Q. Weng, B. Wang, X. Wang, N. Hanagata, X. Li, D. Liu, X. Wang, X. Jiang, Y. Bando and D. Golberg, *ACS Nano*, 2014, **8**, 6123-6130.
50. I.Y. Zhitnyak, I.N. Bychkov, I.V. Sukhorukova, A.M. Kovalskii, K.L. Firestein, D. Golberg, N.A. Gloushankova and D.V. Shtansky, *ACS Appl. Mater. Interfaces.*, 2017, **9**, 32498-32508.

TABLES

Table. 1. Values of lattice parameters and crystallite size for BN nanostructures.

BN nanostructures	Lattice parameters (Å)	Crystallite size (d) (nm)

View Article Online
DOI: 10.1039/C9NJ06029D

	a	c	
Porous BN	2.5037	6.7061	8.81
BN nanosheet	2.5047	6.7203	5.55

View Article Online
DOI: 10.1039/C9NJ06029D

Table. 2. Values of different BET surface area parameters, Total surface area and BET surface area for BN nanostructures.

Adsorbent	A (g/cm^3)	I (g/cm^3)	Q_m (cm^3/g)	C	M (g)	S_{total} m^2	S_{BET} m^2/g
BN nanosheet	0.0199	$9*10^{-5}$	50.0250	222.11	0.0792	217.90	2751.26
Porous BN nanosheet	0.0226	$4*10^{-5}$	44.1696	566.06	0.0765	192.39	2514.90

View Article Online
DOI: 10.1039/C9NJ06029D

Table 3. Kinetic parameters for the adsorption of both the drugs over the surface of BN nanostructures.

Adsorbent	Drug/conc. (mg/L)	Pseudo-first-order model			Pseudo-second-order model		
		q_e (mg/g)	k_1 (min $^{-1}$)	R^2	q_e (mg/g)	K_2(g mg^{-1} min^{-1})	R^2
Porous BN	Levofloxacin/10	0.9855	0.039	0.4957	9.7465	0.2573	0.9999
	Tetracycline/50	12.265	0.0126	0.6896	42.74	0.0057	0.9996
BN nanosheet	Levofloxacin/10	1.4484	0.0587	0.8379	9.6339	0.2307	0.9999
	Tetracycline/50	22.35	0.0161	0.9083	44.052	0.0019	0.9993

(Reaction conditions: pH-4 (Levofloxacin), pH-6 (Tetracycline); BN nanostructures: 1g/L; Drug dosage: 10mg/L (Levofloxacin) and 50mg/L (Tetracycline))

View Article Online
DOI: 10.1039/C9NJ06029D

Table 4. Adsorption isotherm data for the adsorption of both the drugs over the surface of BN nanostructures.

Langmuir isotherm					
Sample	**Drug**	**q_{max} (mg g^{-1})**	**K_L (L mg^{-1})**	**R_L**	**R^2**
Porous BN	**Levofloxacin**	17.6056	2.007	0.047	0.903
	Tetracycline	129.87	0.051	0.285	0.987
BN nanosheet	**Levofloxacin**	20.0803	1.398	0.067	0.981
	Tetracycline	86.206	0.097	0.171	0.985

Freundlich isotherm				
Sample	**Drug**	**n**	**K_F ((mg g^{-1}) (Lmg^{-1})$^{1/n}$)**	**R^2**
Porous BN	**Levofloxacin**	4.472	10.889	0.7645
	Tetracycline	1.771	10.631	0.9499
BN nanosheet	**Levofloxacin**	2.897	10.287	0.9398
	Tetracycline	2.27	13.925	0.9208

(Reaction conditions: pH-4 (Levofloxacin), pH-6 (Tetracycline); BN nanostructures: 1g/L; Drug dosage: 5, 10, 15, 20, 25 mg/L (Levofloxacin) and 25, 50, 75, 100, 125 mg/L (Tetracycline).

View Article Online
DOI: 10.1039/C9NJ06029D

Table 5. Kinetics and Adsorption isotherm data for the adsorption of Curcumin over the surface of porous BN nanosheets.

Kinetics	Qe (mg/g)		R^2		Rate constant	
First-order	22.53		0.8266		k_1= 0.0149 min^{-1}	
Second-order	24.038		0.9996		k_2=0.00379 g mg^{-1} min^{-1}	
Langmuir isotherm				**Freundlich isotherm**		
q_{max} (mg g^{-1})	**K_L (L mg^{-1})**	**R_L**	**R^2**	**n**	**K_F ((mg g^{-1}) (Lmg^{-1})$^{1/n}$**	**R^2**
32.362	0.607	0.0618	0.9942	2.126	10.034	0.8247

(Reaction conditions: pH-5 Adsorbent dosage: 1g/L and Curcumin dosage: 5 mg/L, 15 mg/L, 25 mg/L, 35 mg/L and 50 mg/L)

View Article Online
DOI: 10.1039/C9NJ06029D

FIGURES

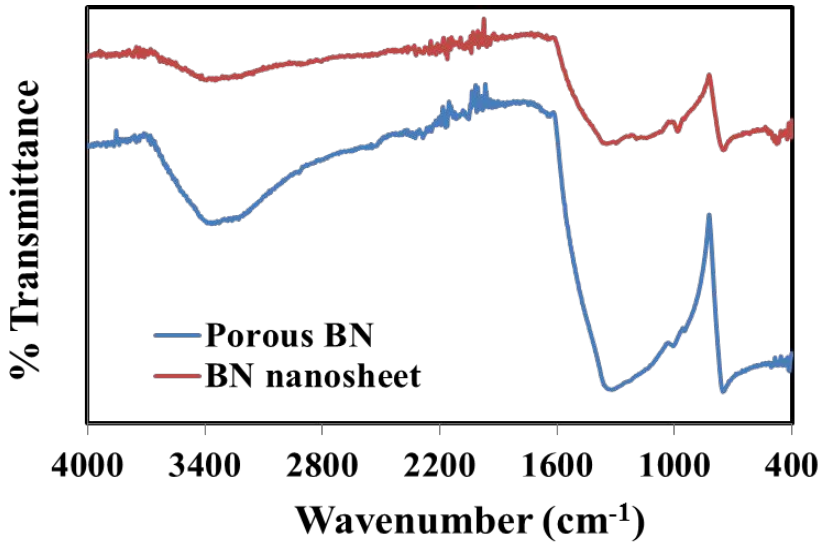

Fig. 1. FT-IR spectra for BN nanostructures.

View Article Online
DOI: 10.1039/C9NJ06029D

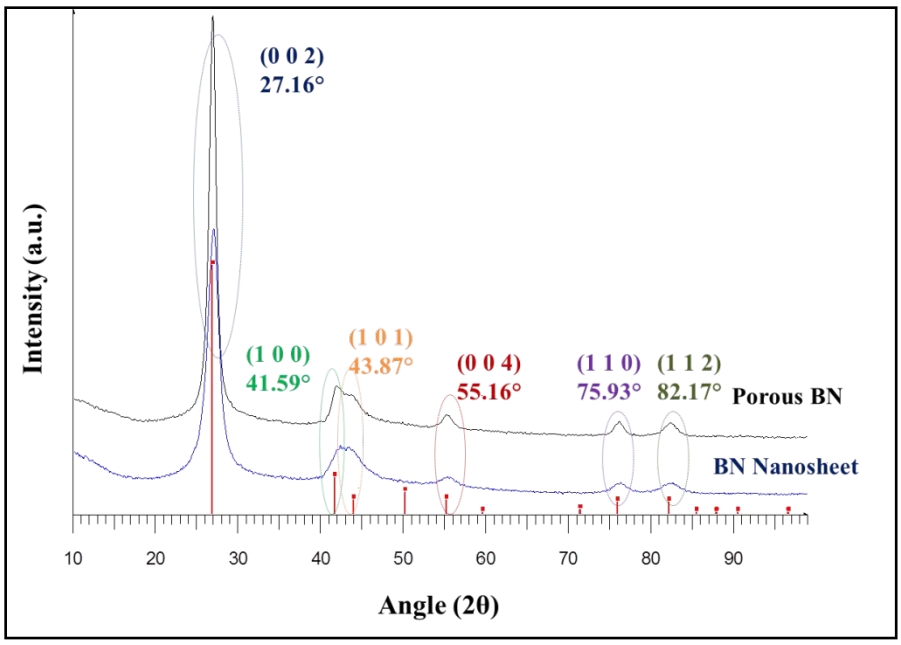

Fig. 2. Powder XRD patterns for BN nanostructures.

View Article Online
DOI: 10.1039/C9NJ06029D

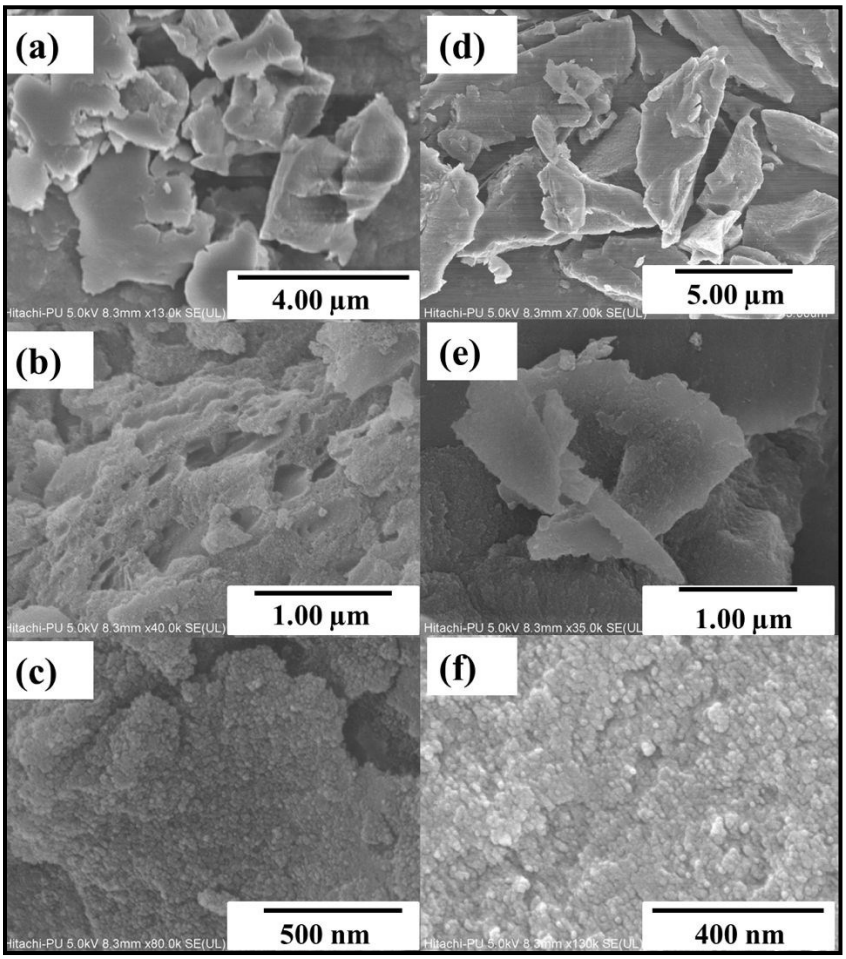

Fig. 3. FE-SEM images for porous BN nanosheet (a,b,c) and BN nanosheet (d,e,f).

View Article Online
DOI: 10.1039/C9NJ06029D

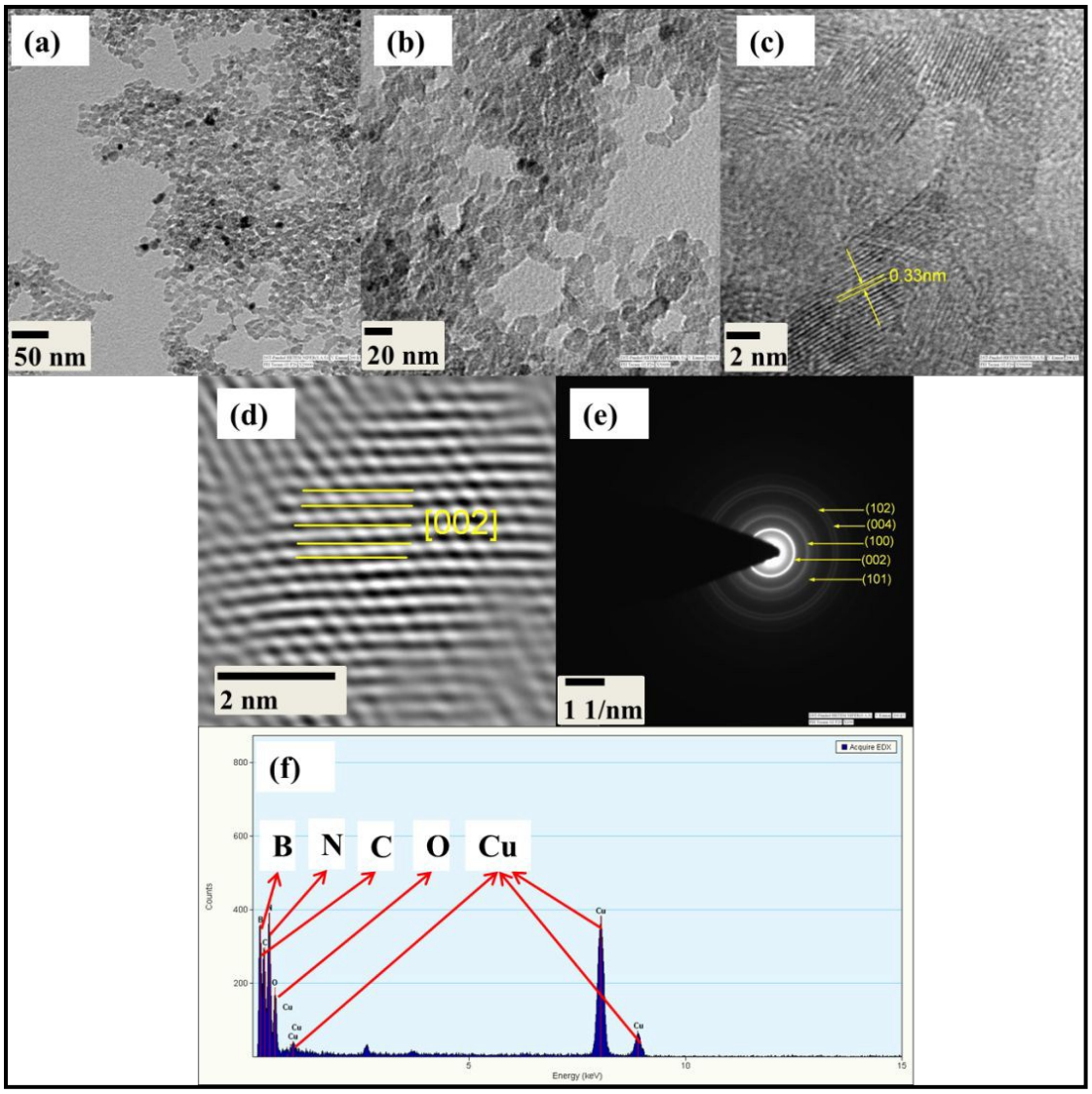

Fig. 4. HR-TEM images for porous BN nanostructures at low resolution (a and b), at high resolution (c and d), SAED pattern (e) and EDS pattern (f).

View Article Online
DOI: 10.1039/C9NJ06029D

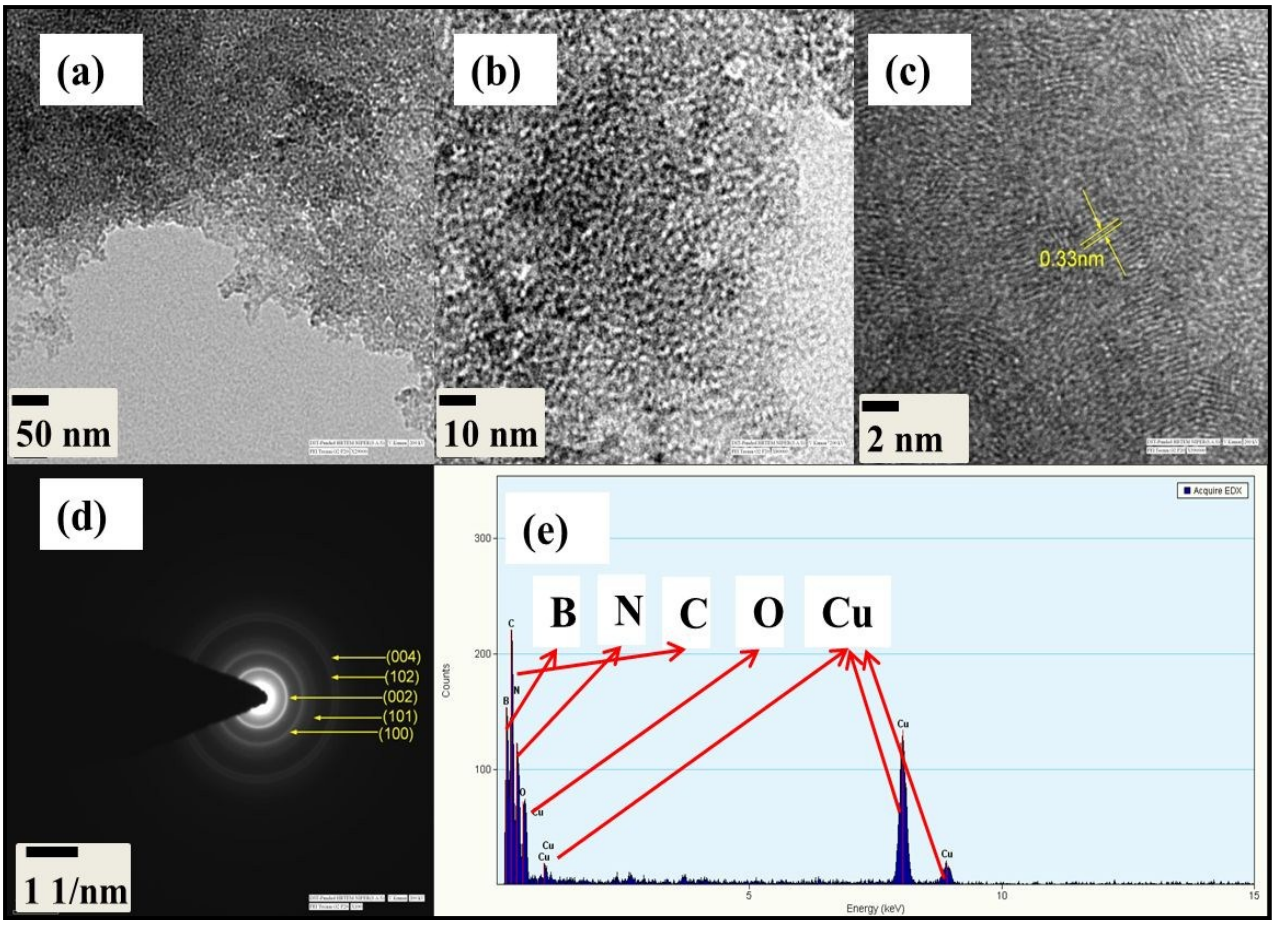

Fig. 5. HR-TEM images for BN nanosheet at low resolution (a and b), at high resolution (c), SAED pattern (d) and EDS pattern (e).

View Article Online
DOI: 10.1039/C9NJ06029D

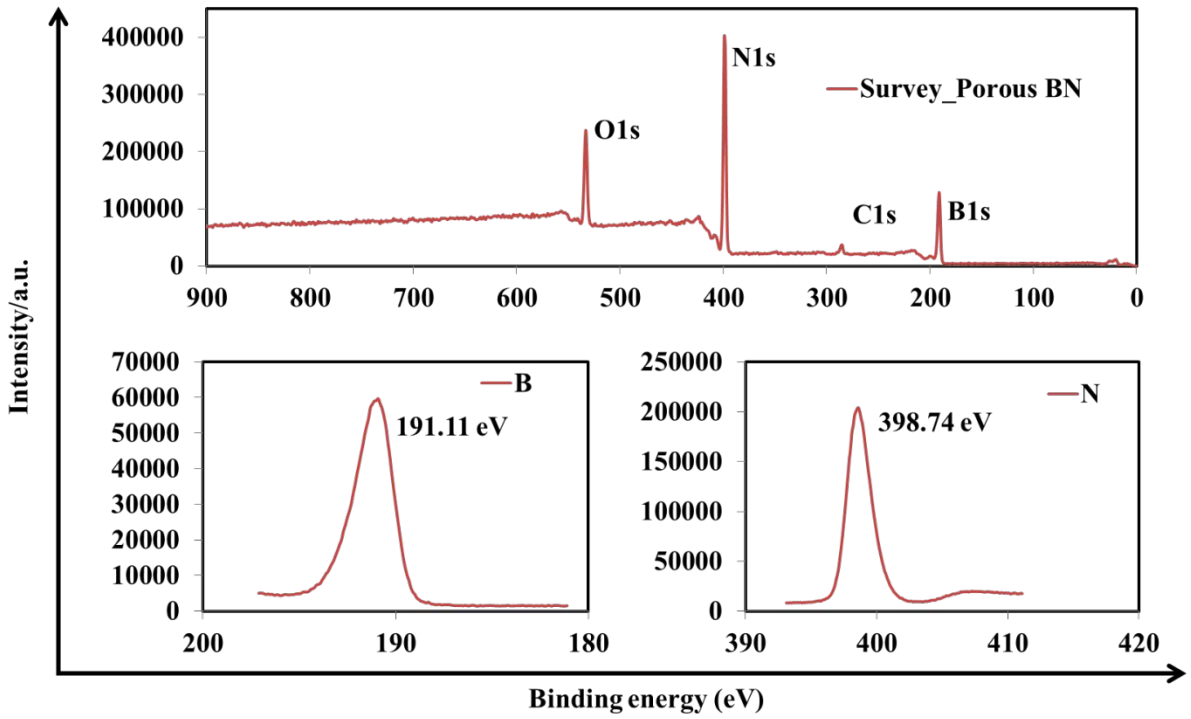

Fig. 6. XPS spectra of the porous BN nanostructures.

View Article Online
DOI: 10.1039/C9NJ06029D

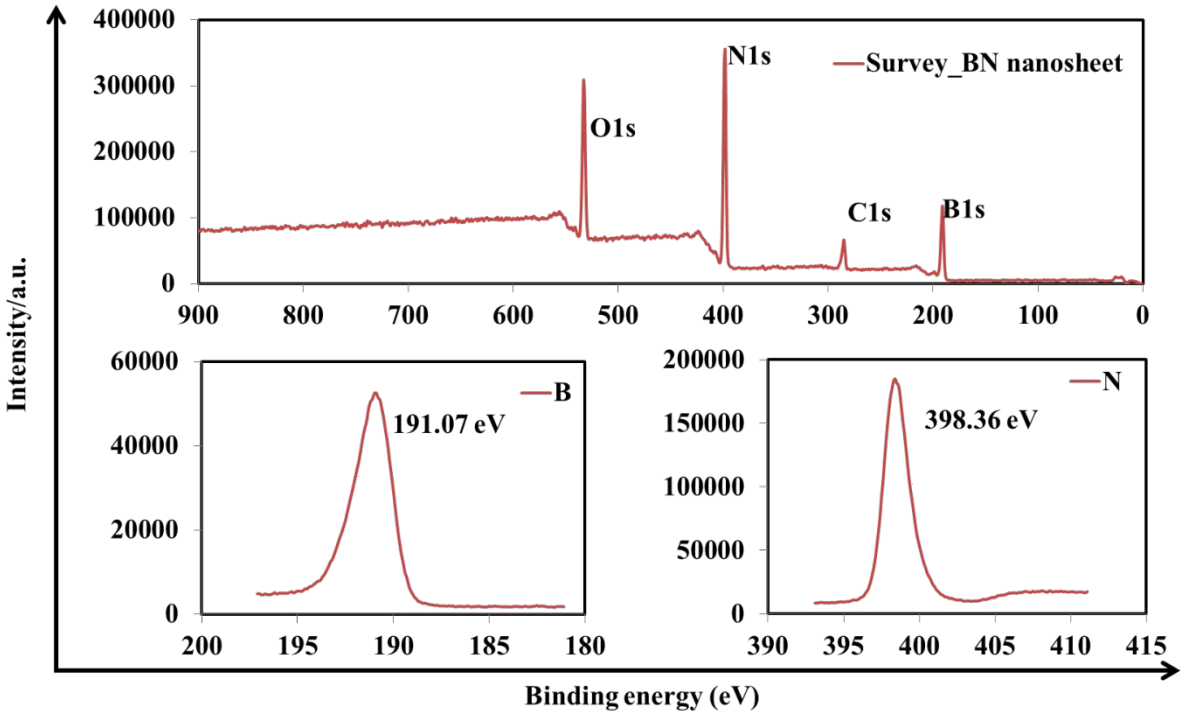

Fig. 7. XPS spectra of the BN nanosheet.

View Article Online
DOI: 10.1039/C9NJ06029D

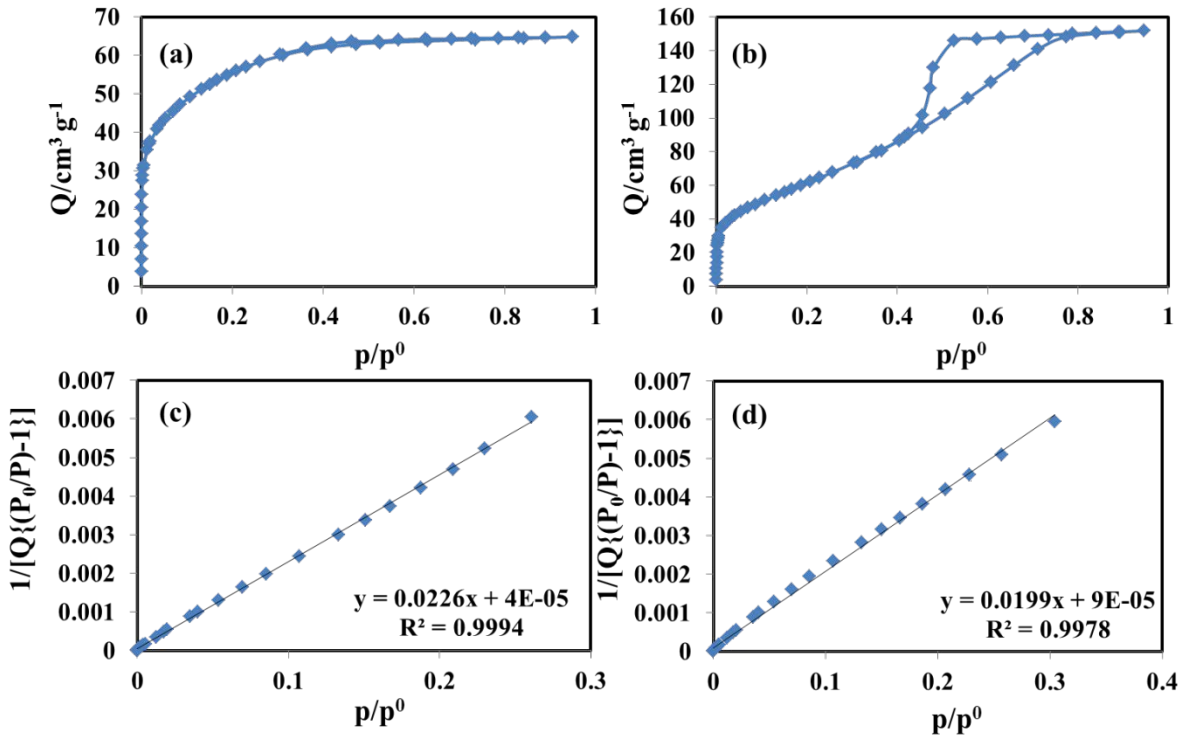

Fig. 8. The N_2 adsorption/desorption isotherms for (a) porous BN nanosheets and (b) BN nanosheets matching with type IV and type I adsorption isotherms and corresponding BET plots (c) and (d).

View Article Online
DOI: 10.1039/C9NJ06029D

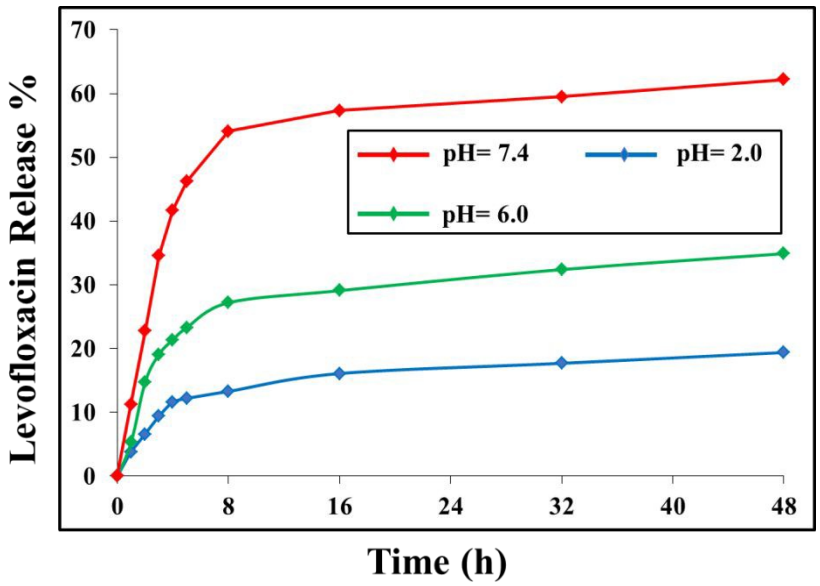

Fig. 9. Release kinetics of Levofloxacin from porous BN-Levofloxacin at different pH values.

View Article Online
DOI: 10.1039/C9NJ06029D

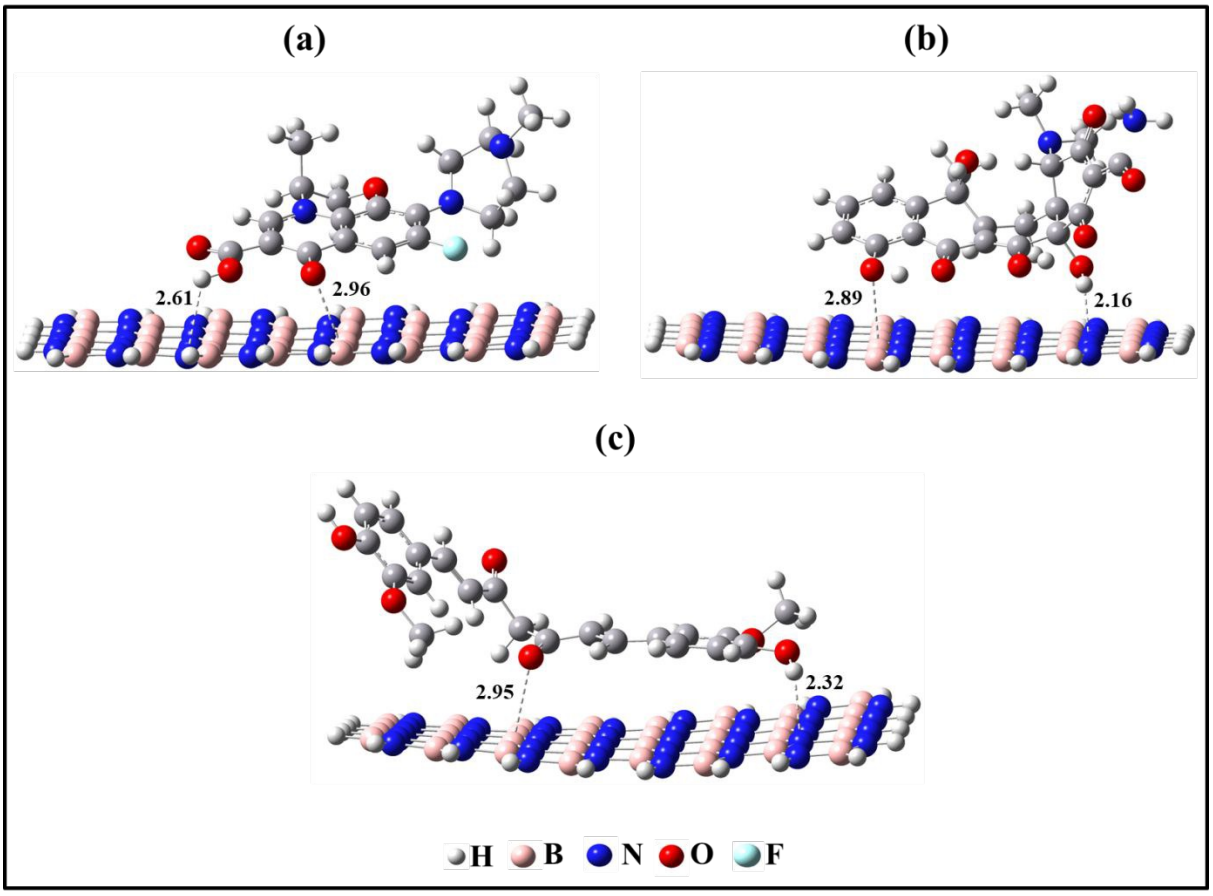

Fig. 10. Optimized structures of (a) Levofloxacin (b) Tetracycline and (c) Curcumin adsorbed over BN nanosheet. (Bond lengths are in Å)

View Article Online
DOI: 10.1039/C9NJ06029D

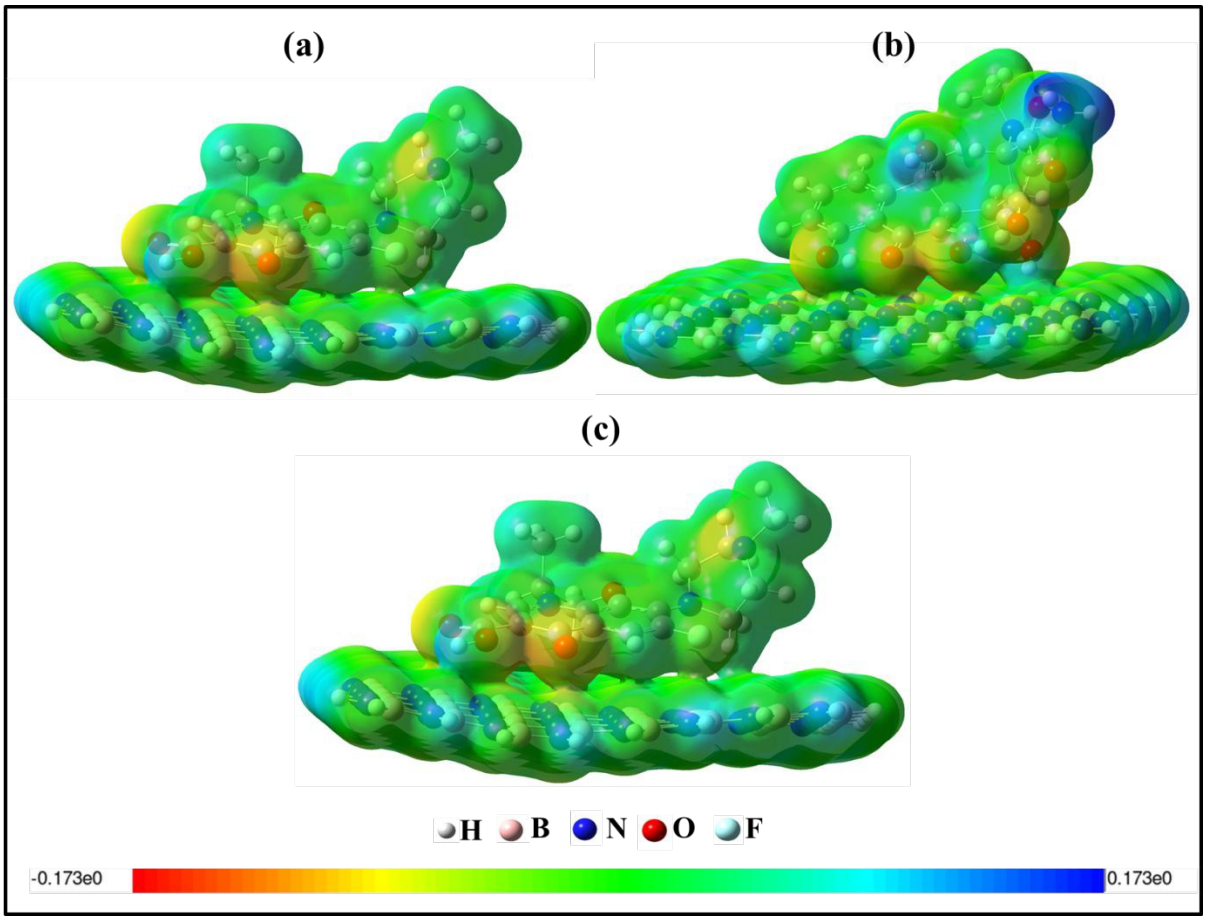

Fig. 11. MEP surfaces of (a) Levofloxacin (b) Tetracycline and (c) Curcumin adsorbed over BN nanosheet.

View Article Online
DOI: 10.1039/C9NJ06029D

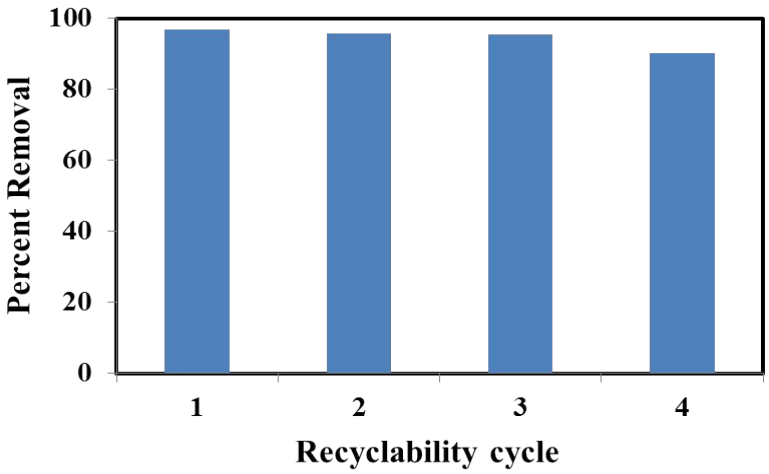

Fig. 12. Recyclability experiment for the adsorption of Levofloxacin over porous BN. (Reaction conditions: pH-4; BN nanostructures: 1g/L; Drug dosage: 10mg/L.

View Article Online
DOI: 10.1039/C9NJ06029D

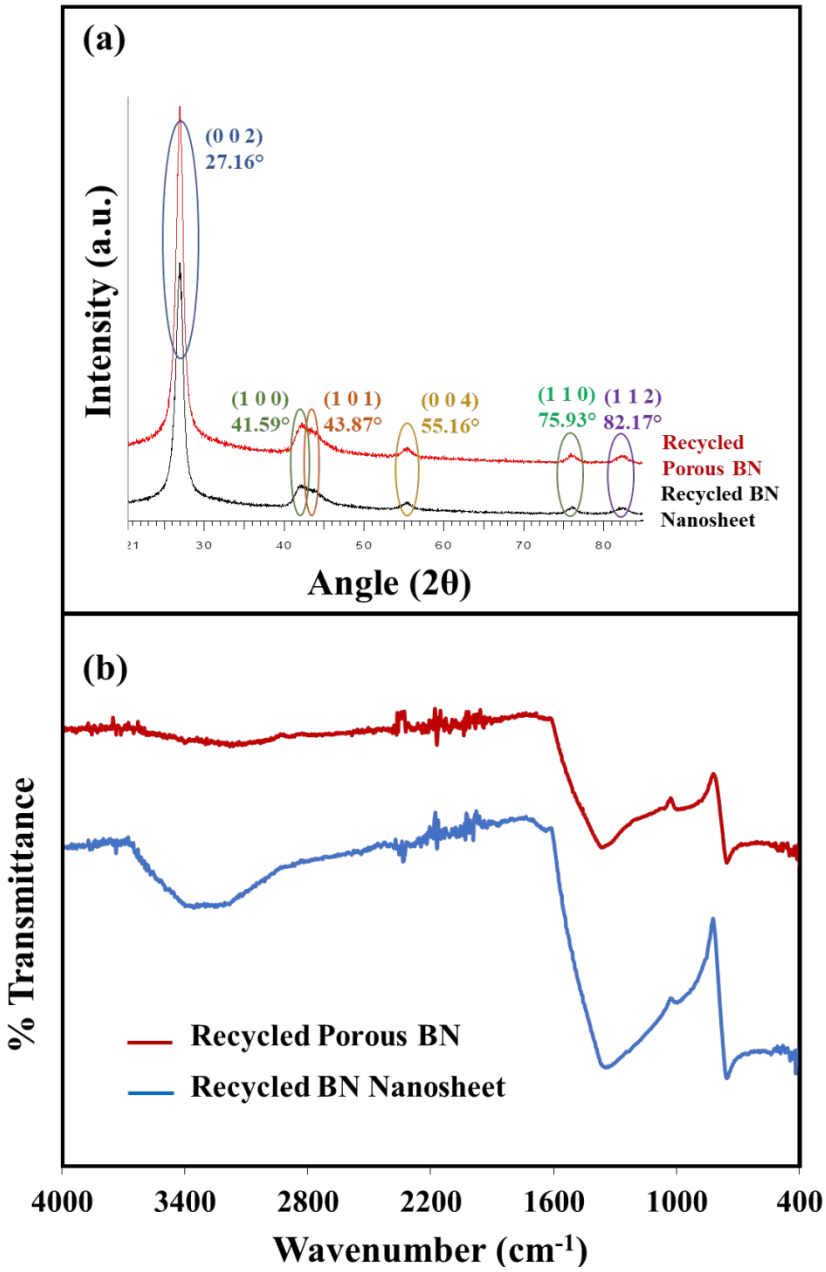

Fig. 13. (a) Powder XRD patterns and (b) FT-IR spectra for recycled BN nanostructures.

View Article Online
DOI: 10.1039/C9NJ06029D

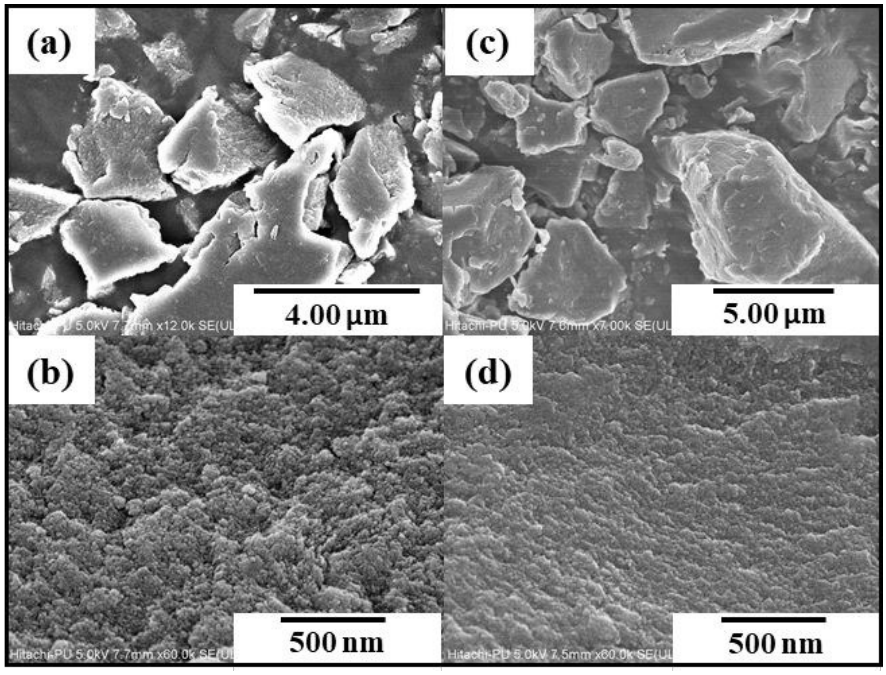

Fig. 14. FE-SEM images for recycled porous BN nanosheet (a,b) and recycled BN nanosheet (c,d).

View Article Online
DOI: 10.1039/C9NJ06029D

Graphical abstract

The biocompatible BN nanosheets were employed as proficient applicants for the effective adsorption of pharmaceutical drugs owing to the high adsorption capacity of BN nanosheets and the favorable interactions between BN and drug molecules.